E-5. Boundary perturbation methods[1]

E-5-1. Lateral boundary perturbation by GSV

To make the lateral boundary perturbation for the GSV method, the global ensemble prediction is first conducted with the T63L40 GSM using the initial perturbations by the GSV method. Three-hourly perturbations from FT=0 to 36 are extracted from the ensemble forecast by subtracting the control run forecast. Detailed procedures are described in E-4-2.

E-5-2. Lateral boundary perturbation by WEP

To make the lateral boundary perturbation for other 4 methods (WEP, MSV, MBD and LET), the JMA operational one-week EPS was adopted as in the WEP initial perturbation method. Perturbations from the JMA operational one-week EPS were extracted by subtracting the control run forecast from the first 5 positive ensemble members. Forecast data of the JMA operational one-week EPS are transferred daily to MRI through the exclusive line. However, since the highest level of the archived pressure plane forecast GPV (RSMC Tokyo responsible area) is located at 100 hPa and is lower than the model top of the 40 level NHM (22.1 km ~ 40 hPa), the RSMC forecast GPVs were first interpolated to the 32 level hybrid NHM (NHM L32) model planes (model top is located at 13.8 km ~ 160 hPa), and perturbations are extracted by subtracting the interpolated field of the control run from perturbed runs. Then, the perturbations are normalized and added to the lateral boundary condition of the control run of 40 level hybrid NHM (NHM L40). In the highest 8 levels of the NHM L40, perturbation at the 32nd level of the NHM L32 was extrapolated. At the *kz*-th level, the amplitude of perturbation was multiplied by the following coefficient *c1*:

$$c1 = \frac{1 - \cos\{\pi * (kz - 32)/8\}}{2}, \qquad \text{(E-5-1)}$$

so that the perturbation amplitude becomes zero at the model top of the NHM L40. Similar procedure has been employed in the Myanmar cyclone Nargis' ensemble prediction (Saito et al, 2010; see G-4 and Fig. G-4-1), but in case of Nargis' EPS, not the RSMC Tokyo EPS data of 6 hourly 12 levels but global EPS forecast data of 12 hourly 11 levels were used.

Since the timing of the file transfer of the RSMC Tokyo forecast GPVs from NPD to MRI is too late to conduct the near real time EPS run of B08RDP, the RSMC Tokyo forecast data at 12 UTC one day before was used. The amplitude of global EPS perturbation was adjusted considering the difference of initial times. To evaluate forecast errors of the JMA's operational global EPS, the evolution of ensemble spread of the 500 hPa height filed (Fig. E-5-1) was adopted. Spread of WEP was defined by a function WEPSPR (FT), and the amplitude of global EPS perturbation at the forecast time FT=*iftg* (24-60 hours) was adjusted by multiplying the following coefficient *c2*:

[1] Contents of this section are submitted as Saito et al. (2010c).

$$c2 = \frac{WESPR(ifrt)}{WEPSPR(iftg)}, \tag{E-5-2}$$

where *iftr* is the forecast time of mesoscale ensemble prediction (0-36 hours). After the adjustment of amplitude, perturbations are interpolated in time and space, and added to the 3 hourly 40 km L40 lateral boundary conditions for NHM produced from the high resolution GSM forecast (see E-3-5). The saturation adjustment was applied to all perturbed lateral boundary conditions.

Similar lateral boundary perturbations were prepared with a horizontal resolution of 40 km for breeding cycles in MBD and forecast analysis cycle in LET (see E-5-4 and E-5-5).

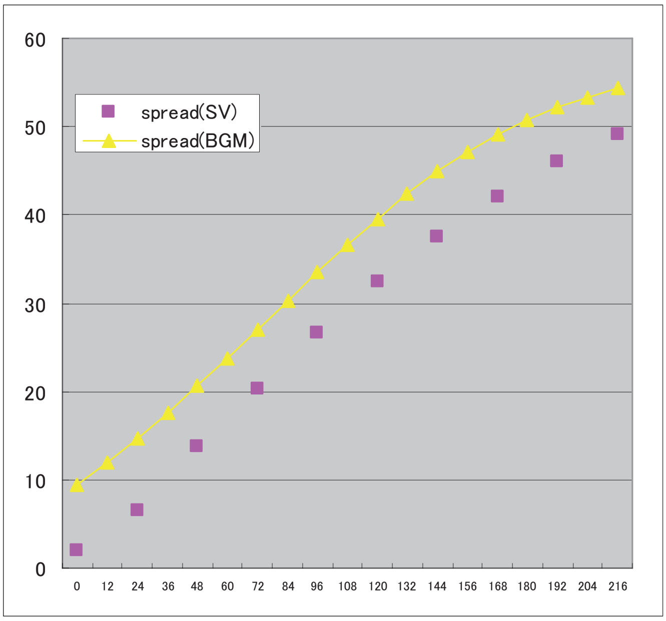

Fig. E-5-1. Evolution of statistical ensemble spread of the 500 hPa height filed in the JMA's global one-week EPS. Spread (BGM) indicated by triangles is before October 2007, while Spread (SV) by squares is after November 2007 and this function was used in the 2008 experiment. Courtesy of Ryouta Sakai of NPD/JMA.

E-5-3. Perturbation for soil temperature

Perturbation for soil temperature was applied to the 2008 experiment using the GSV method with the same manner as in the 2007 experiment (D-5).

E-5-4. Effect of lateral boundary perturbations in MBD

In this subsection, the effect of lateral boundary perturbations in MBD and LET methods is discussed. Figure E-5-2 shows the forecast of the control run with the initial time of 12 UTC 4 July 2008. The initial condition is given by Meso 4DVAR application (E-3-1) and the lateral boundary condition is given by the GSM forecast of JMA (E-3-5). In this case, a synoptic disturbance was located in the southwest of Beijing at initial time (Fig. E-5-2a; FT=3). This low pressure system moved northeastward and reached northeast of Beijing at 12 UTC on 5 July (Fig. E-5-2b; FT=24).

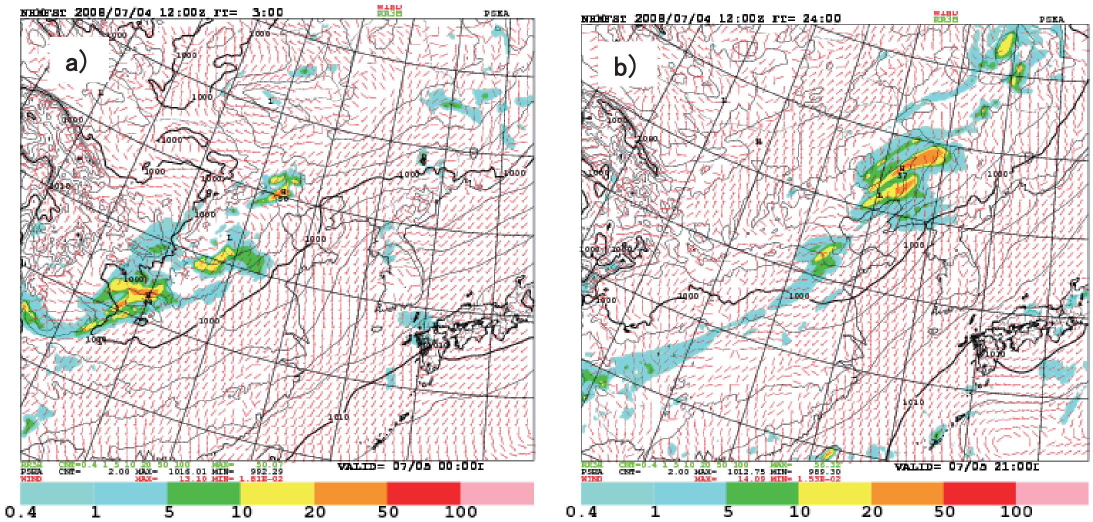

Fig. E-5-2. Sea level pressure and accumulated 3 hour precipitation predicted by the control run. Initial time is 12 UTC 4 July 2008. a) FT=3. b) FT=24.

a. Pure effect of lateral boundary perturbations only

First we examine the ensemble characteristics purely due to the lateral boundary perturbation only. Figure E-5-3 shows horizontal distribution of ensemble spread of temperature and horizontal wind at 850 hPa. Even without initial perturbations if we apply the lateral perturbation to the forecast, ensemble spread soon increases near the lateral boundaries at FT=3 (Figs. E-5-3a and b), and the influence of the lateral boundary perturbation propagates inside of the model domain. Eventually the spread grows around the synoptic disturbance (Figs. E-5-3c and d).

Figure E-5-4a shows the evolution of ensemble spreads of surface field in the common verification area (105~125°E, 30~45°N; see Fig. D-2-1). Needless to say, ensemble spread is zero at the initial time without the initial perturbation but it gradually increases with time. Spread of the surface pressure increases rapidly, because pressure difference propagates with the speed of sound waves. Spreads increase almost linearly during the 36 hour forecast period and reach about 1 m/s for horizontal wind (V), 0.8 hPa for surefire pressure, 0.5 C for temperature and 3 % for relative humidity. Spread of 3 hour accumulated rain (RR3H) decreases after FT=27, but this is attributable to the passage of the low pressure system. RMSEs of the ensemble mean are almost the same or slightly smaller than those of the control run (Fig. E-5-3b). This result shows that the lateral boundary perturbations are properly implemented and contribute to improve the accuracy of the ensemble forecast.

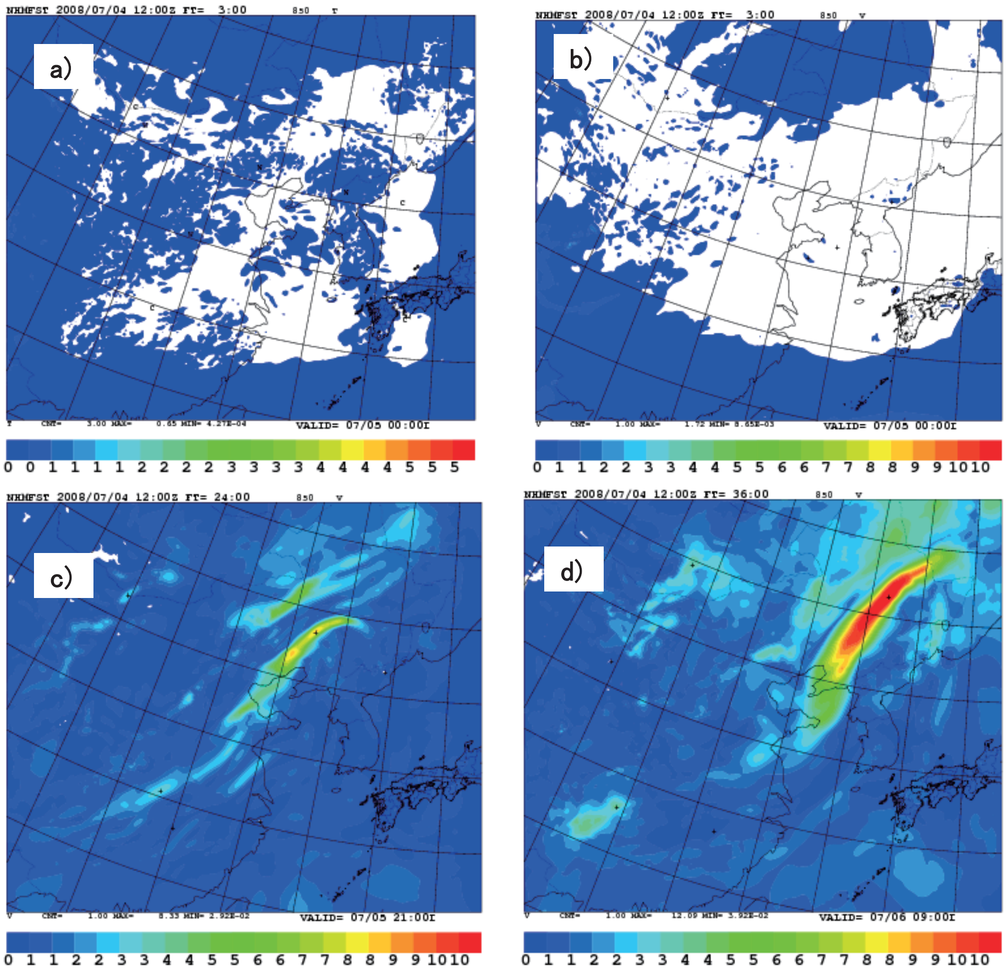

Fig. E-5-3. Ensemble spread of T at 850 hPa in the experiment with lateral boundary perturbation only (no initial perturbation). Initial time is 12 UTC 4 July 2008. a) Temperature at FT=3. b) Horizontal wind (V) at FT=3. c) Same as b) but FT=24. d) FT=36.

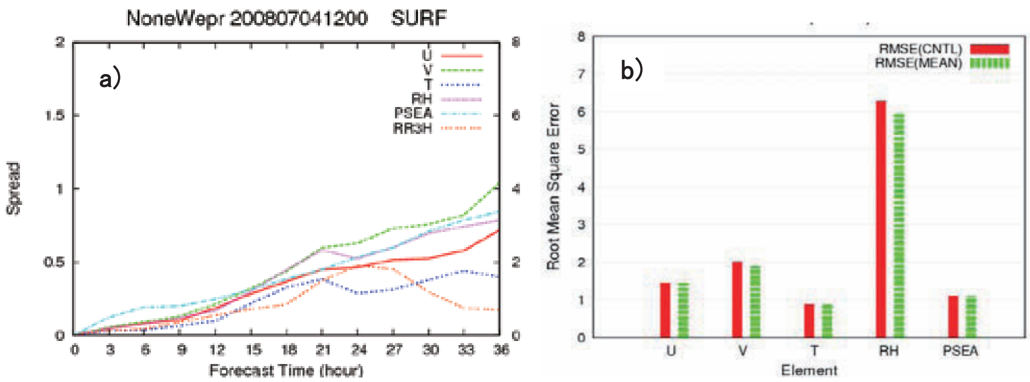

Fig. E-5-4. a) Time sequence of the 11 member ensemble spreads of surface elements in the common verification area in the experiment with the lateral boundary perturbation only. Initial time is 12 UTC 4 July 2008. b) Horizontal wind (V) at FT=3. c) RMS errors of ensemble means at FT=24 against the initial condition. (analysis at 12 UTC 5 July). Red bars show RMSEs by control run (CNTL) while green bars show those by ensemble mean.

b. Ensemble forecast without the lateral boundary perturbation[2]

Figure E-5-5 shows horizontal distribution of ensemble spread of horizontal wind at 850 hPa in the MBD experiment without the lateral boundary perturbation. Without the lateral boundary perturbation, bred vectors cannot grow near the lateral boundaries and the initial perturbation is confined inside of the model domain (Fig. E-5-5a). Ensemble spread remains small and even slightly decreases near the lateral boundaries in the forecast period. At FT=36, spread is small and grows only around the synoptic disturbance (Fig. E-5-5b).

Figure E-5-6 shows the ensemble spread of surface elements. The growth is slow and reaches the upper limit after FT=24. Spread of the surface temperature becomes largest in the day time (FT=12-21), corresponding to the diurnal change.

Figure E-5-7 indicates 3 hour accumulated precipitation at 12UTC 5 July (FT=24) predicted by the ensemble prediction. Result by each member resembles each other. Ensemble spread (lower right) of precipitation is confined in the area of the ensemble mean, which suggest that the spread is mainly given by the difference of intensity, and the positional difference is small.

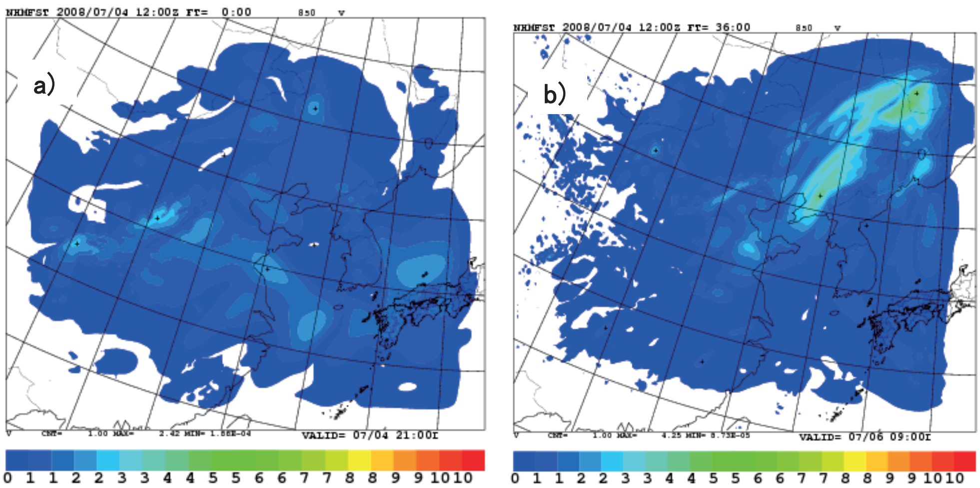

Fig. E-5-5. Ensemble spread horizontal wind (V) at 850 hPa in the MBD experiment without lateral boundary perturbation. Initial time is 12 UTC 4 July 2008. a) at FT=0. b) at FT=36.

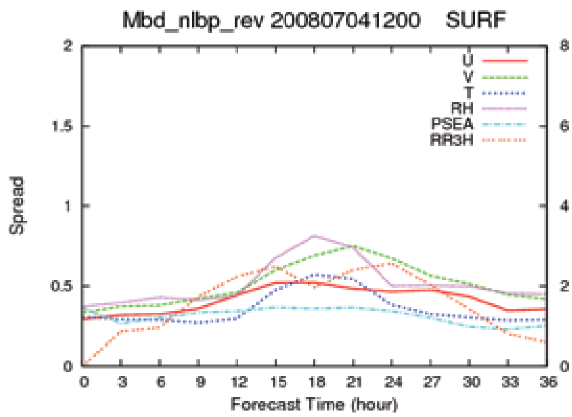

Fig. E-5-6. Same as Fig. E-5-4a but in the MBD experiment without lateral boundary perturbations.

[2] Results in the subsections hereafter are based on the re-computations of the 2008 experiment (E-4-6b).

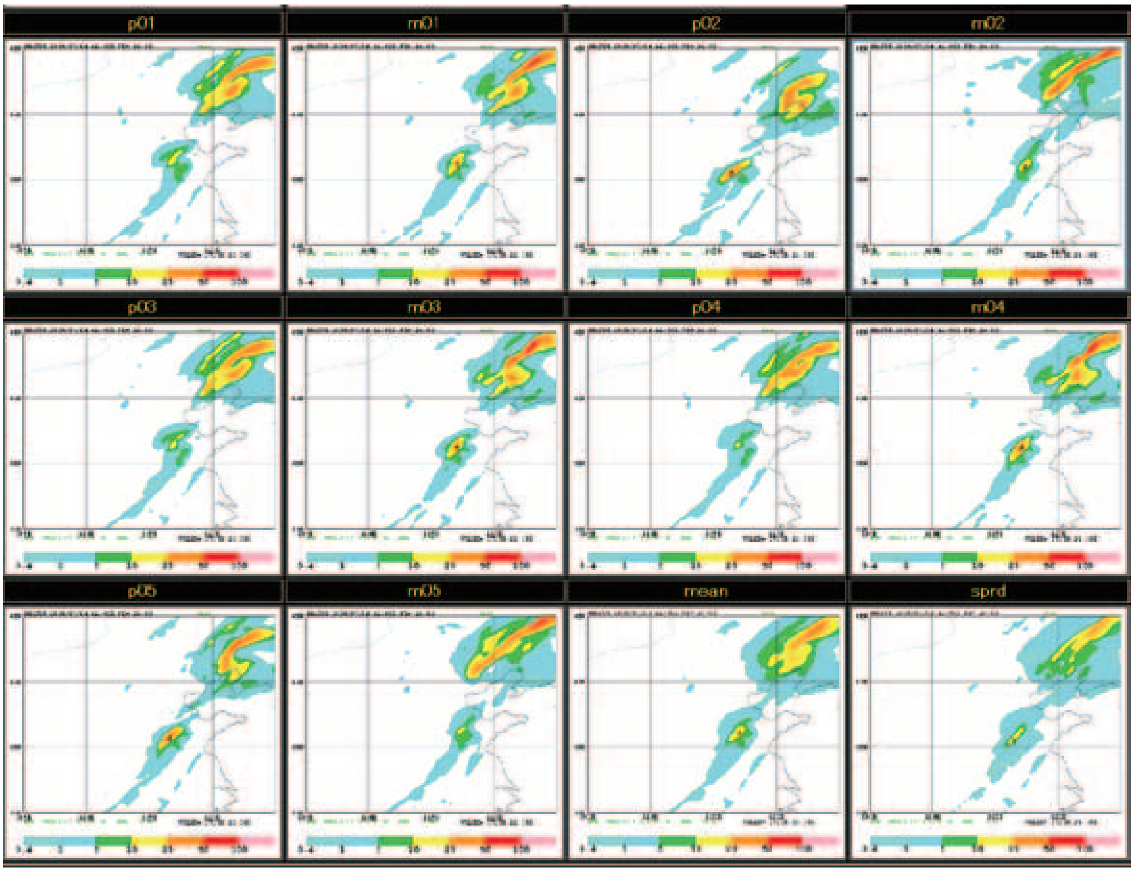

Fig. E-5-7. 3 hour accumulated precipitation at 12UTC 5 July (FT=24) predicted by each member, ensemble mean and ensemble spread. Case of the MBD method without LBC perturbations.

c. Effect of lateral boundary perturbations in the ensemble forecast

When the lateral perturbation was implemented in the forecast period, ensemble spreads in the later half (after FT=18) become larger. Figure E-5-8 shows horizontal distribution of ensemble spread of horizontal wind at 850 hPa in the MBD experiment when the lateral boundary perturbation was implemented. Compared to the result without the lateral boundary perturbation (Fig. E-5-5b), ensemble spread extends throughout the model domain and the amplitude of spread around the disturbance becomes larger. However, Fig. E-5-8b is similar to Fig. E-5-4b, which means that bred initial perturbation does not grow enough in the latter half of the forecast period and at FT=36 the influence of the lateral boundary perturbation is dominant. This fact is confirmed by the figure of RMSEs (Fig. E-5-9). RMSEs in the MBD method with lateral boundary perturbations are larger than those without lateral boundary perturbations (Fig. E-5-6) in the latter half of the forecast period, however at FT=36, their magnitudes are almost the same as in the experiment only with the lateral boundary perturbation (Fig. E-5-4).

Figure E-5-10 indicates 3 hour accumulated precipitation at 12UTC 5 July (FT=24) predicted by the ensemble prediction with lateral boundary perturbations. Compared with the case of no lateral boundary perturbation (Fig. E-5-7), result by each member differs each other. Ensemble spread (lower right) of precipitation extends to wider areas.

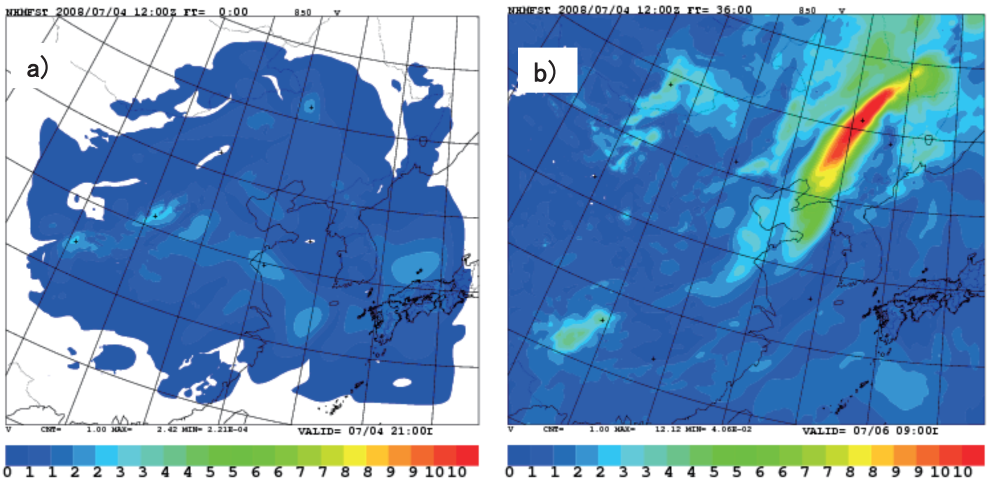

Fig. E-5-8. Same as Fig. E-5-5 but with lateral boundary perturbations.

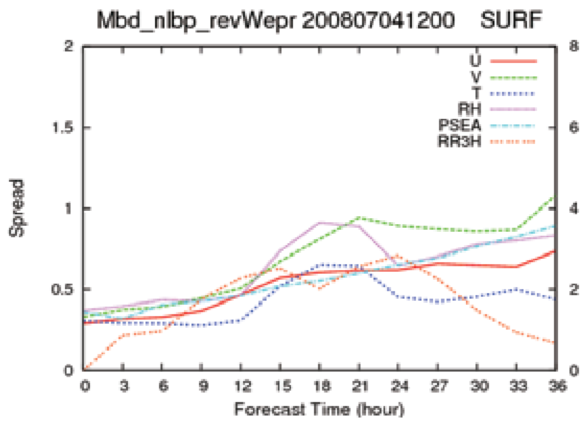

Fig. E-5-9. Same as Fig. E-5-6 but with lateral boundary perturbations.

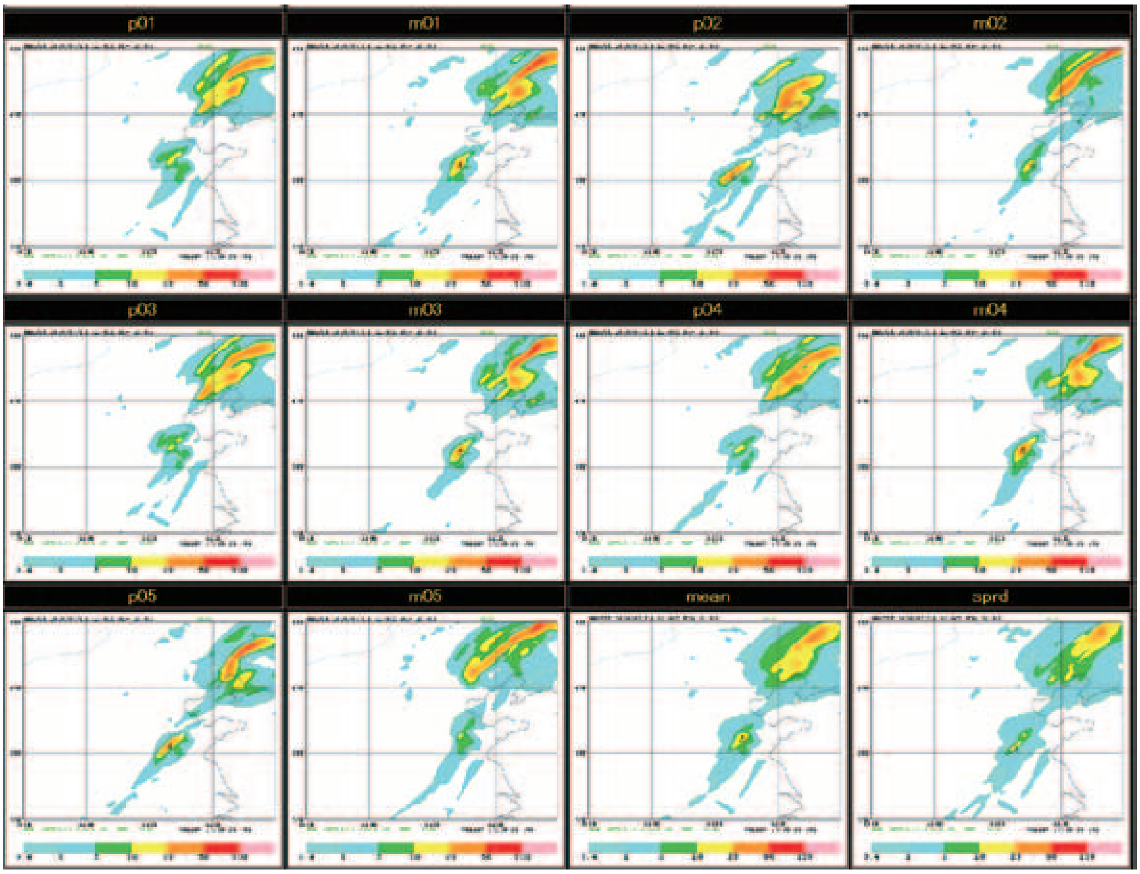

Fig. E-5-10. Same as in Fig. E-5-7. Case of the MBD method with LBC perturbations in the forecast.

d. Effect of lateral boundary perturbations in breeding cycles

Lateral boundary perturbations were applied not only to the ensemble forecast with a horizontal resolution of 15 km but also to the breeding cycles with a horizontal resolution of 40 km. Similar procedures described in E-5-2 were taken to the 6 hourly breeding cycle using the global EPS forecast GPV of the day before (2 July 2008).

Figure E-5-11 is the horizontal distribution of ensemble spread of horizontal wind (V) at 850 hPa level corresponding to Fig. E-5-8. The bred initial perturbations at FT=0 (Fig. E-5-11a) spread over the whole forecast domain and their amplitudes become larger. Compared with Fig. E-5-8a, location of initial spread shifts southwestward and positional correspondence with the synoptic disturbance also improved. This effect continues throughout the forecast period of 36 hours. At FT=36 (Fig. E-5-11b), the spread is larger and more solid compared to Fig. E-5-8b. Time sequence of ensemble spreads is shown in Fig. E-5-12. Spreads become larger from the early stage of the forecast, and continue to increase throughout the forecast period. Diurnal changes are seen in the spreads of the surface temperature and relative humidity, and the changes become more distinct. This result means that difference of diurnal change is simulated in each ensemble member more properly. Magnitudes of ensemble spreads at FT=36 are much larger than Fig. E-5-9. Interestingly, the difference of spread amplitude at FT=36 between Fig. E-5-12 and Fig. E-5-9 (difference of boundary perturbation in breeding cycles) is larger than the difference between Fig. E-5-9 and Fig. E-5-6 (difference with and without initial perturbations). These results show the importance of lateral boundary perturbations in the breeding cycle to make proper bred vectors (initial perturbations).

Figure E-5-13 indicates 3 hour accumulated precipitation at 12UTC 5 July (FT=24) corresponding to Fig. E-5-10. Appearance of each member has its own individuality. Ensemble spread extends further than Fig. E-5-10.

Averaged RMSEs for 2 days from 3 to 4 July 2008 for surface elements are shown in Fig. E-5-14. Implementation of lateral boundary perturbations in breeding cycle contributes not only to increase the ensemble spread but to improve the accuracy of the ensemble forecast. Upper level verifications are shown in Figs. E-5-15 (850 hPa), E-5-16 (500 hPa) and E-5-17 (250 hPa). Importance of lateral boundary perturbations in the breeding cycle is obvious.

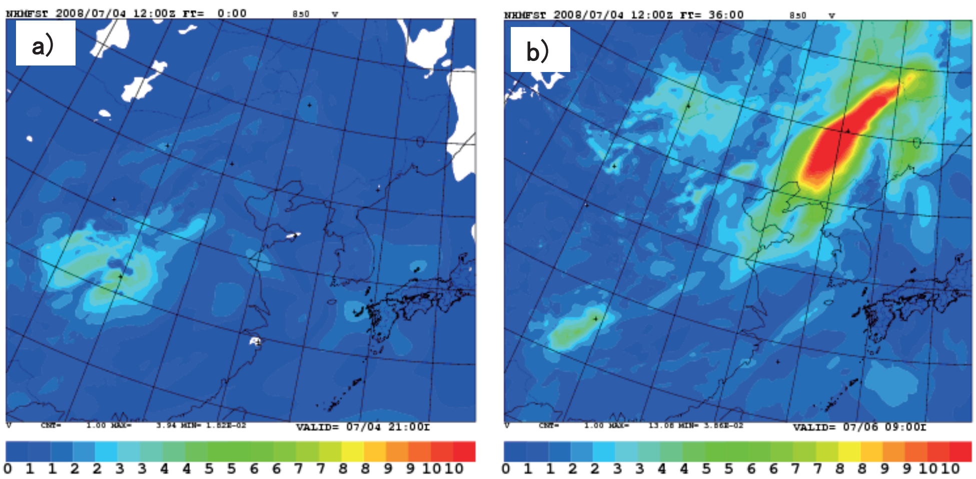

Fig. E-5-11. Same as Fig. E-5-8 but with lateral boundary perturbations in both breeding cycles and the ensemble forecast.

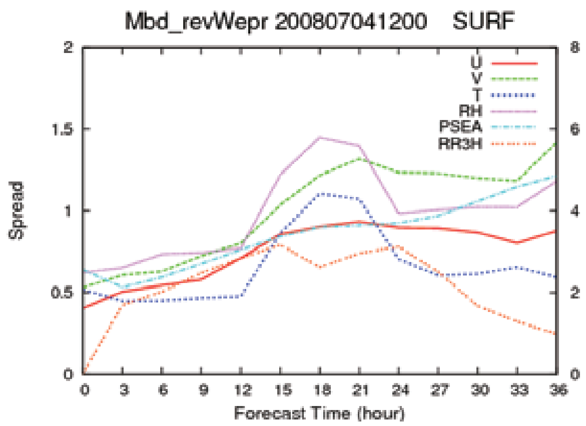

Fig. E-5-12. Same as Fig. E-5-9 but with lateral boundary perturbations in both breeding cycles and the ensemble forecast.

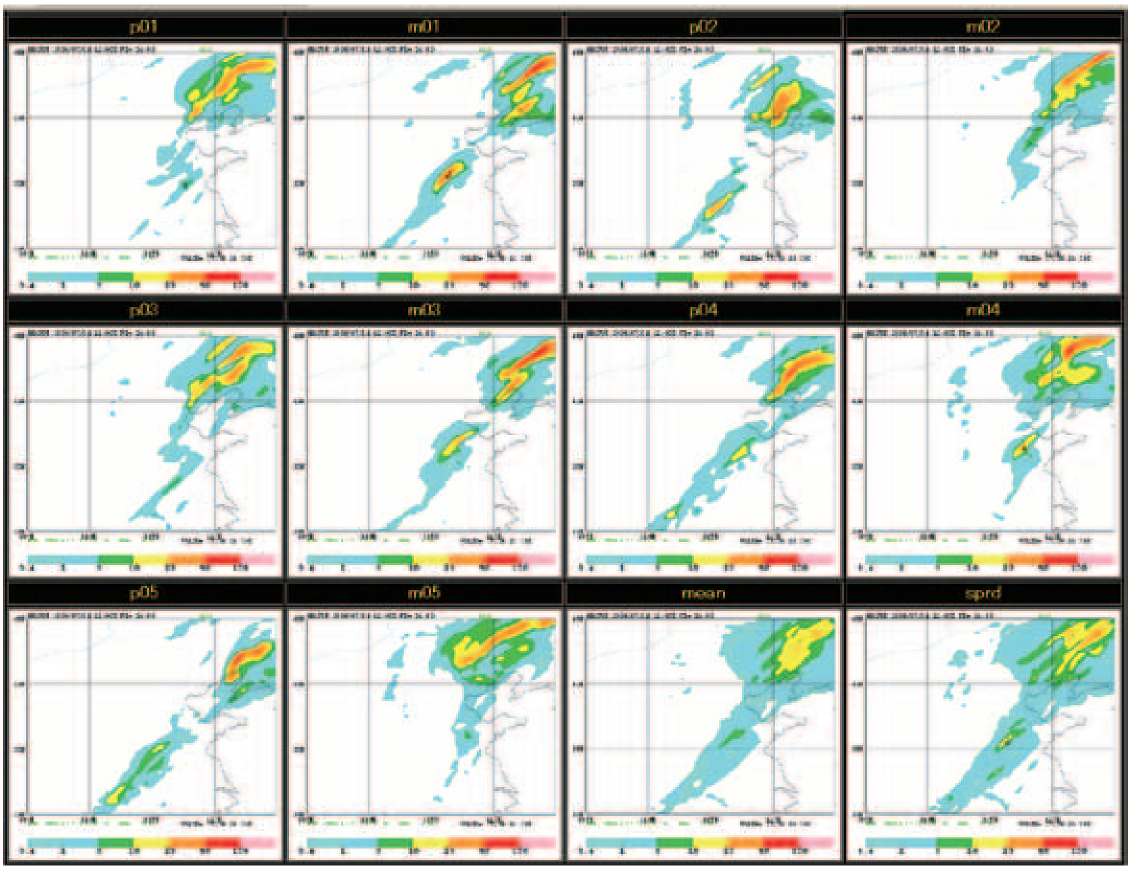

Fig. E-5-13. Same as in Fig. E-5-10. Case of the MBD method with LBC perturbations in both breeding cycles and ensemble forecast.

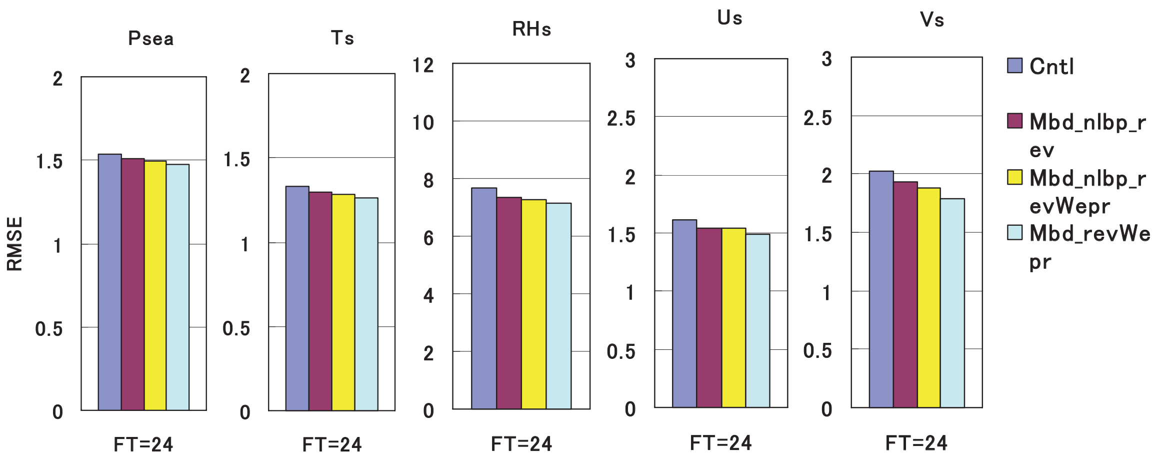

Fig. E-5-14. Averaged RMSEs against initial conditions in the 2 days of 3 and 4 July 2008 for surface elements. From left to right, mean sea level pressure, 2 m temperature, 2 m relative humidity, 10 m horizontal wind (U and V). Mbd_nlbp_rev is no lateral boundary perturbations, Mbd_nlbp_revWep is lateral boundary perturbations in the forecast, and Mbd_revWep is the result with lateral boundary perturbations both in the breeding cycle and the extended forecast.

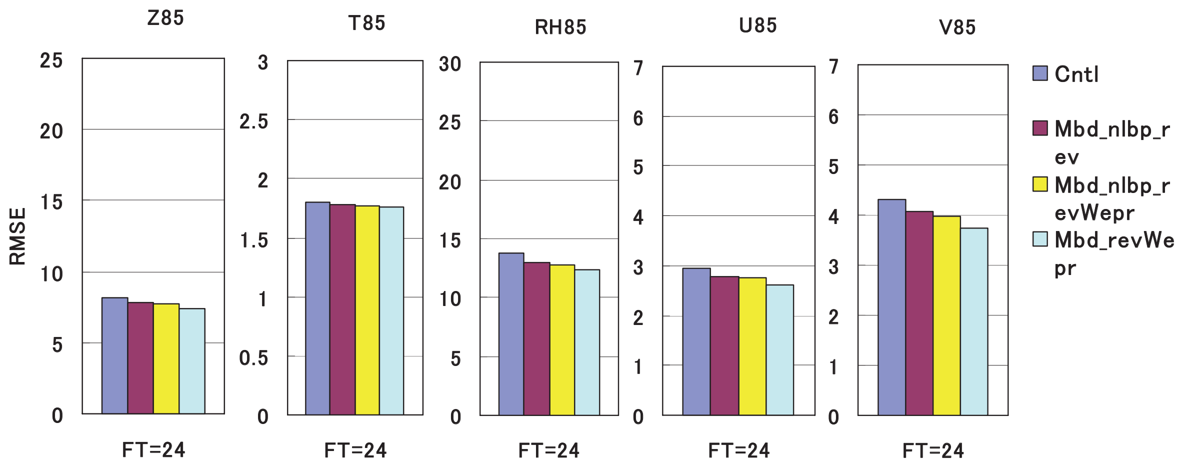

Fig. E-5-15. Same as in Fig. E-5-14 but elements at 850 hPa level. Z85 is height field.

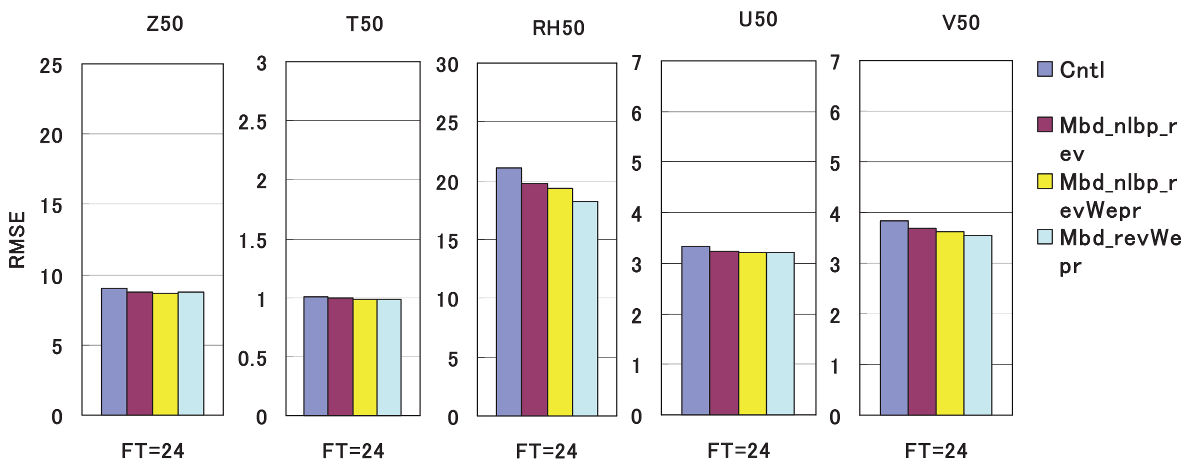

Fig. E-5-16. Same as in Fig. E-5-14 but elements at 500 hPa level.

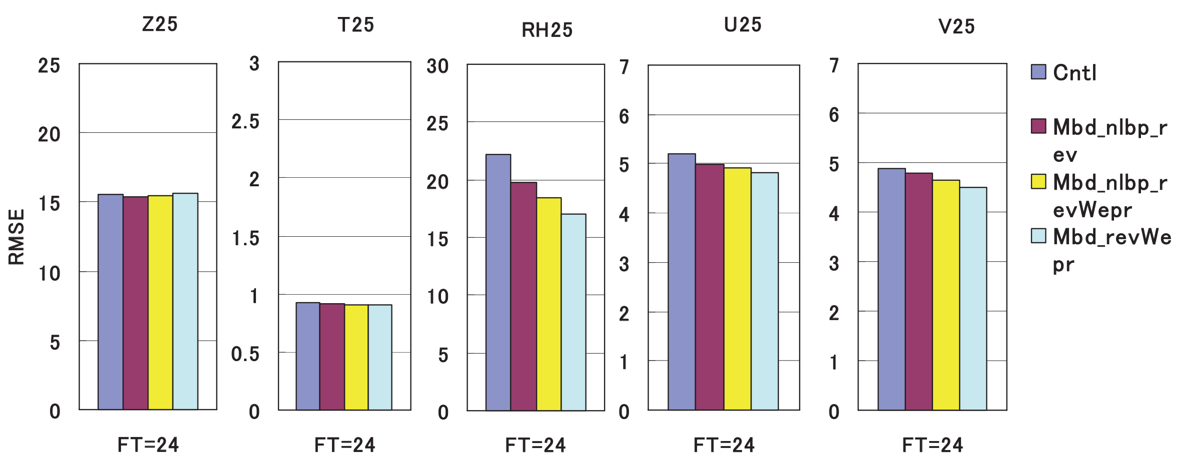

Fig. E-5-17. Same as in Fig. E-5-14 but elements at 250 hPa level.

e. Similarity index

To see the reason of improvement of the ensemble forecast performance by applying the lateral boundary perturbations in breeding cycles, similarity indexes between initial perturbations were computed. Norm operator of the similarity index was defined by the moist total energy norm (D-4-1). Table E-5-1 shows the indexes for the case of no lateral boundary perturbations in breeding cycles. Here, from p1 to p5 are positive perturbations and from m1 to m5 are negative perturbations. Since negative perturbations are given by subtracting the bred vector, their directions are opposite to the positive perturbation of same numbers but slightly deformed by the saturation adjustment thus the indexes between positive and negative perturbations with same number are almost -1.0 (indicated with blue shade). As depicted with yellow shade numerals in this table, some bred vectors are similar (similarity index is larger than 0.4, e.g., angle between the two vectors is less than 66 degrees) to each other.

Table. E-5-1. Similarity index between bred vectors. In the case without lateral boundary perturbations in breeding cycles.

	p1	p2	p3	p4	p5	m1	m2	m3	m4	m5
p1	1.00	0.25	0.50	0.18	0.21	−1.00	−0.25	−0.49	−0.18	−0.21
p2	0.25	1.00	0.04	0.02	0.62	−0.25	−0.99	−0.03	−0.01	−0.61
p3	0.50	0.04	1.00	0.65	−0.05	−0.49	−0.03	−0.99	−0.64	0.06
p4	0.18	0.02	0.65	1.00	−0.18	−0.18	0.00	−0.64	−0.98	0.19
p5	0.21	0.62	−0.05	−0.18	1.00	−0.20	−0.61	0.06	0.19	−0.99
m1	−1.00	−0.25	−0.49	−0.18	−0.20	1.00	0.25	0.50	0.19	0.21
m2	−0.25	−0.99	−0.03	0.00	−0.61	0.25	1.00	0.03	0.00	0.62
m3	−0.49	−0.03	−0.99	−0.64	0.06	0.50	0.03	1.00	0.65	−0.06
m4	−0.18	−0.01	−0.64	−0.98	0.19	0.19	0.00	0.65	1.00	−0.19
m5	−0.21	−0.61	0.06	0.19	−0.99	0.21	0.62	−0.06	−0.19	1.00

Table. E-5-2. Same as Table E-5-1. In the case with lateral boundary perturbations in breeding cycles.

	p1	p2	p3	p4	p5	m1	m2	m3	m4	m5
p1	1.00	0.09	0.39	0.21	−0.07	−0.99	−0.08	−0.37	−0.20	0.07
p2	0.09	1.00	0.28	0.03	0.53	−0.08	−0.98	−0.26	−0.02	−0.52
p3	0.39	0.28	1.00	0.20	0.00	−0.37	−0.25	−0.97	−0.18	0.02
p4	0.21	0.03	0.20	1.00	0.25	−0.21	−0.02	−0.19	−0.99	−0.24
p5	−0.07	0.53	0.00	0.25	1.00	0.07	−0.52	0.01	−0.24	−0.99
m1	−0.99	−0.08	−0.37	−0.21	0.07	1.00	0.08	0.37	0.21	−0.07
m2	−0.08	−0.98	−0.25	−0.02	−0.52	0.08	1.00	0.27	0.02	0.53
m3	−0.37	−0.26	−0.97	−0.19	0.01	0.37	0.27	1.00	0.19	−0.01
m4	−0.20	−0.02	−0.18	−0.99	−0.24	0.21	0.02	0.19	1.00	0.24
m5	0.07	−0.52	0.02	−0.24	−0.99	−0.07	0.53	−0.01	0.24	1.00

Table E-5-2 shows the similarity indexes for the case when lateral boundary perturbations are implemented in breeding cycles. The number of similar vector pair is drastically decreased, which means the orthogonality of each vector is improved. Improvement of ensemble forecast accuracy (decrease of RMSEs) by lateral boundary perturbations in breeding cycles is partly attributable to this effect.

E-5-5. Effect of lateral boundary perturbations in LETKF

Similar experiments as in the former subsection were applied to the LET method (E-4-5). Forecast analysis cycle is 6 hourly and horizontal resolution is 40 km as in the MBD method. Since the effect of lateral boundary perturbations in the ensemble forest should be similar to the result of MBD, lateral boundary perturbations are applied to the extended forecast and their effect in the data assimilation cycle is examined[3].

a. Ensemble forecast with lateral boundary perturbations

Figure E-5-18 shows horizontal distribution of ensemble spread of horizontal wind at 850 hPa in the LET experiment when the lateral boundary perturbations were implemented in the extended forecast. Since lateral boundary perturbations were omitted in the LETKF forecast analysis cycle in this experiment, initial spreads (Fig. E-5-18a) are small near the lateral boundaries. At FT=36, the large spread area moved northward, corresponding to the low pressure system (Fig. E-5-18b). These distributions of ensemble spread are very similar to those by the MBD method (Fig. E-5-8) except that the amplitude of LET is slightly smaller than MBD. We can see that the initial perturbations of LET are smaller than MBD over Japan and around Beijing, where the observation density is high. This indicates that in LET, observation density is reflected to the initial perturbation amplitude.

Figure E-5-19 shows the evolution of ensemble spreads of surface field in the common verification area. Characteristics of spreads in this figure are similar to the corresponding results by MBD (Fig. E-5-9), but the diurnal change in temperature and relative humidity is somewhat smaller than that in MBD. Spreads at FT=36 are almost the same as in Figs. E-5-4a and E-5-9.

Figure E-5-20 indicates 3 hour accumulated precipitation at 12UTC 5 July (FT=24) predicted by the ensemble prediction. Compared with Fig. E-5-8, ensemble spread is slightly smaller than MBD, and the result by each member is somewhat similar to the ensemble mean.

[3] Results in this subsection were obtained by re-computations of the 2008 experiment (E-4-6b).

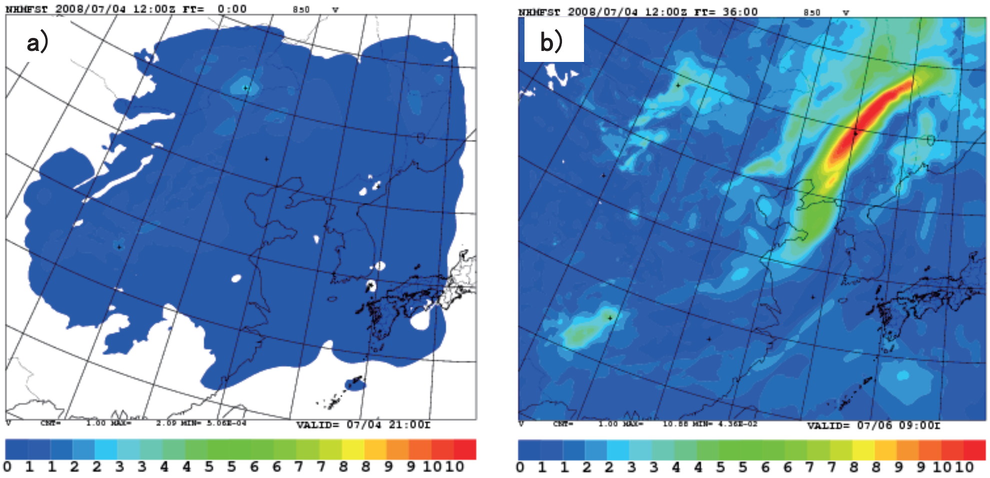

Fig. E-5-18. Same as Fig. E-5-8 but LETKF perturbations.

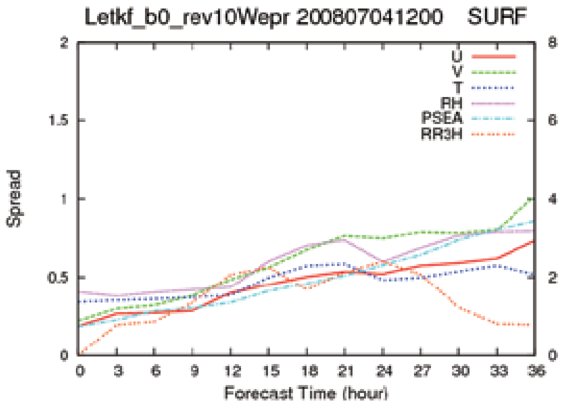

Fig. E-5-19. Same as Fig. E-5-9 but LET method.

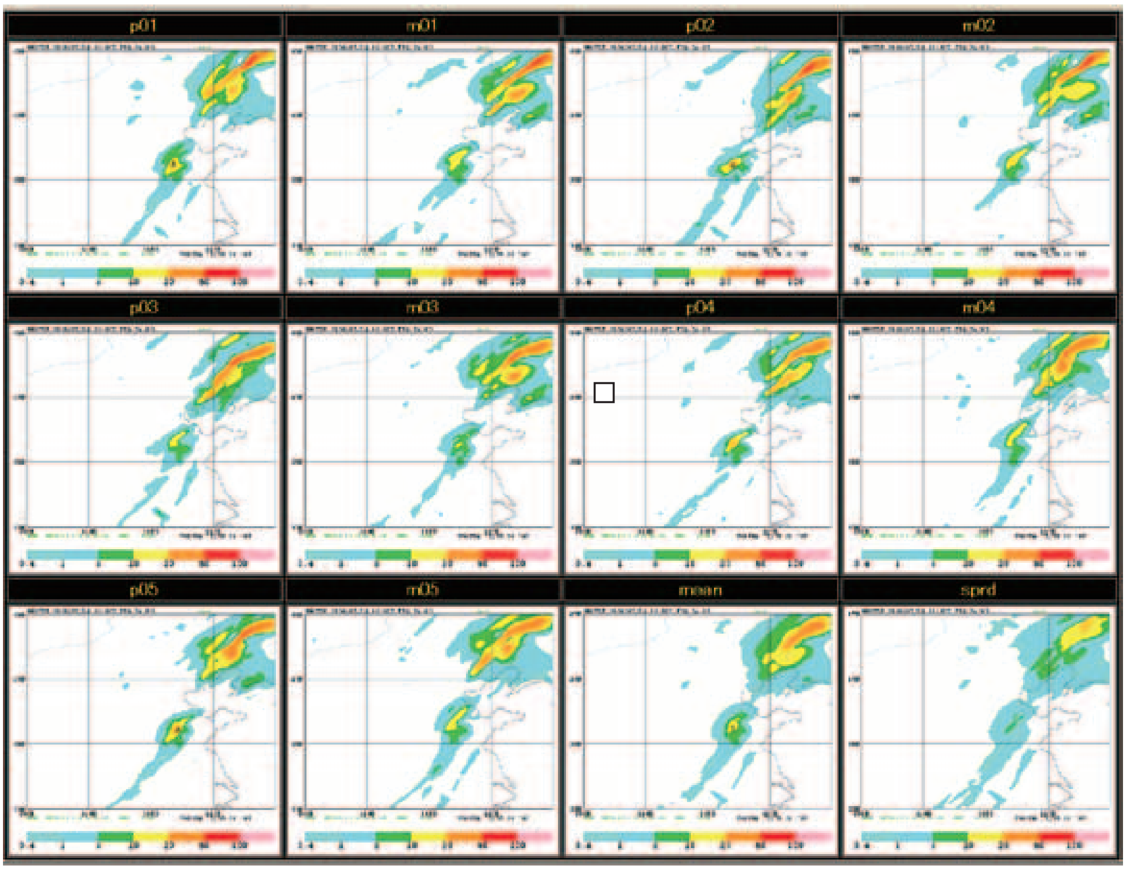

Fig. E-5-20. Same as in Fig. E-5-10. Case of the LET method with LBC perturbations in the forecast.

b. Effect of lateral boundary perturbations in LETKF forecast analysis cycles on ensemble prediction

Lateral boundary perturbations were applied not only to the ensemble forecast with a horizontal resolution of 15 km but also to the LETKF forecast analysis cycles with a horizontal resolution of 40 km. Similar procedures described in E-5-4 were taken to the 6 hourly forecast analysis cycle of LETKF from 30 June 2008.

Figure E-5-21 shows the horizontal distribution of ensemble spread of horizontal wind (V) at 850 hPa level corresponding to Figs. E-5-5 and E-5-11. The analyzed initial perturbations at FT=0 (Fig. E-5-21a) spread over whole forecast domain and their amplitude become larger. Compared with Fig. E-5-18a, location of initial spread shifts southwestward and positional correspondence with the synoptic disturbance also improved. Note that the initial perturbations are still smaller over Japan and around Beijing, where the observation density is high. Compared with the MBD result (Fig. E-5-11a), in LET, the observation density is reflected to the initial perturbation amplitude. The effect in initial perturbations continues throughout the forecast period of 36 hours. At FT=36 (Fig. E-5-21b) compared to the result Fig E-5-18b, the spread is larger and more solid, though somewhat smaller than those of MBD.

The evolution of ensemble spreads is shown in Fig. E-5-22a. Spreads become larger from the early stage of the forecast, and continue to increase throughout the forecast period. Diurnal changes become clearer than Fig. E-5-19, but smaller than those of MBD (Fig. E-5-12). Magnitudes of ensemble spreads at FT=36 are much larger than Fig. E-5-19, but slightly smaller than Fig. E-5-12.

Figure E-5-23 indicates 3 hour accumulated precipitation at 12UTC 5 July (FT=24) corresponding to Fig. E-5-20. Individuality of each member is increased, though ensemble spread is slightly smaller than Fig. E-5-10.

Averaged RMSEs in the 2 days from 3 to 4 July 2008 for surface and 500 hPa elements are shown in Figs. E-5-24 and E-5-25. Implementation of lateral boundary perturbations in EnKF cycles contributes not only to increase the ensemble spread but to improve the accuracy of the ensemble forecast. RMSEs of ensemble mean decrease by the implementation of lateral boundary perturbations in the forecast analysis cycle. Compared with the corresponding MBD case (Figs. E-5-14 and E-5-16), RMSEs by LETKF are slightly larger than MBD.

These results show the importance of lateral boundary perturbations in the LETKF forecast analysis cycle to make the initial perturbations better.

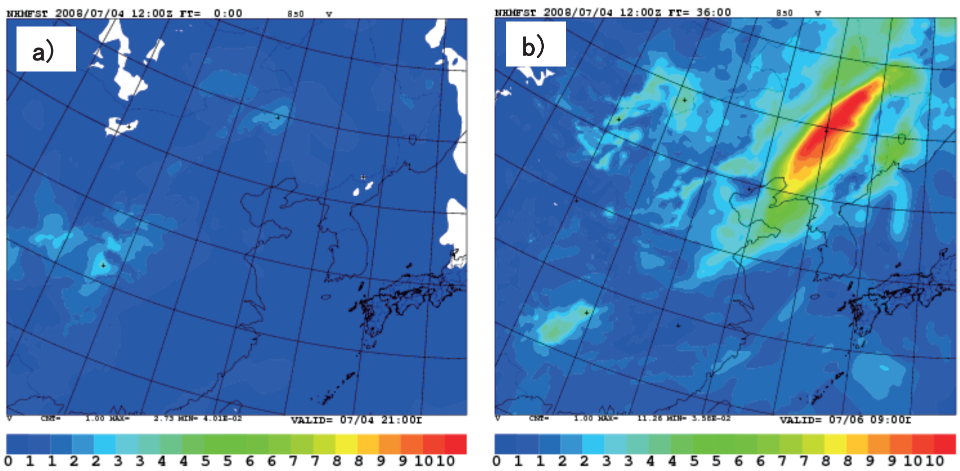

Fig. E-5-21. Same as Fig. E-5-18 but with lateral boundary perturbations in both forecast analysis cycles and the ensemble forecast.

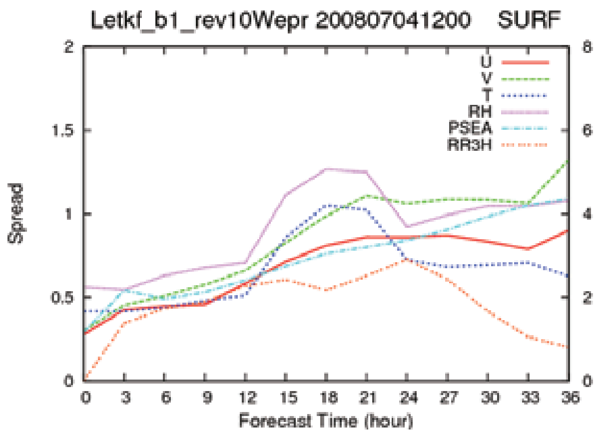

Fig. E-5-22. Same as Fig. E-5-19 but with lateral boundary perturbations in both forecast analysis cycles and the ensemble forecast.

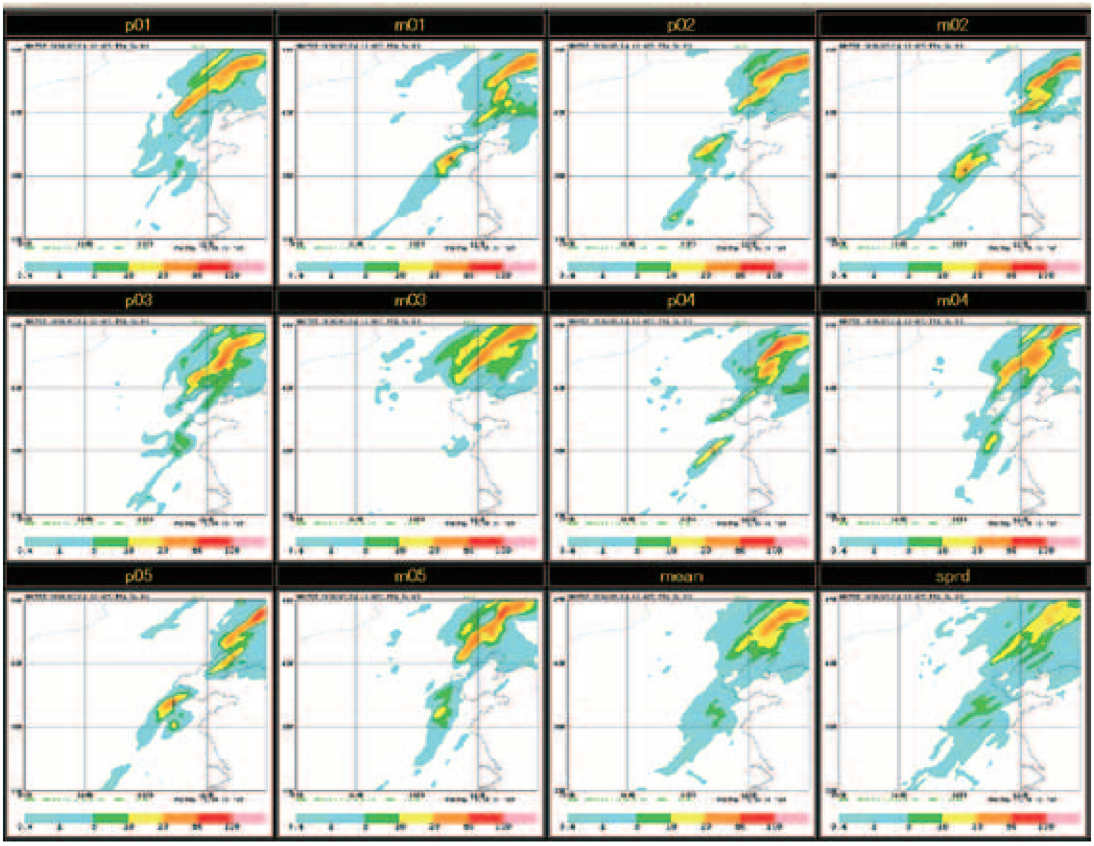

Fig. E-5-23. Same as Fig. E-5-18 but with lateral boundary perturbations in both forecast analysis cycles and the ensemble forecast.

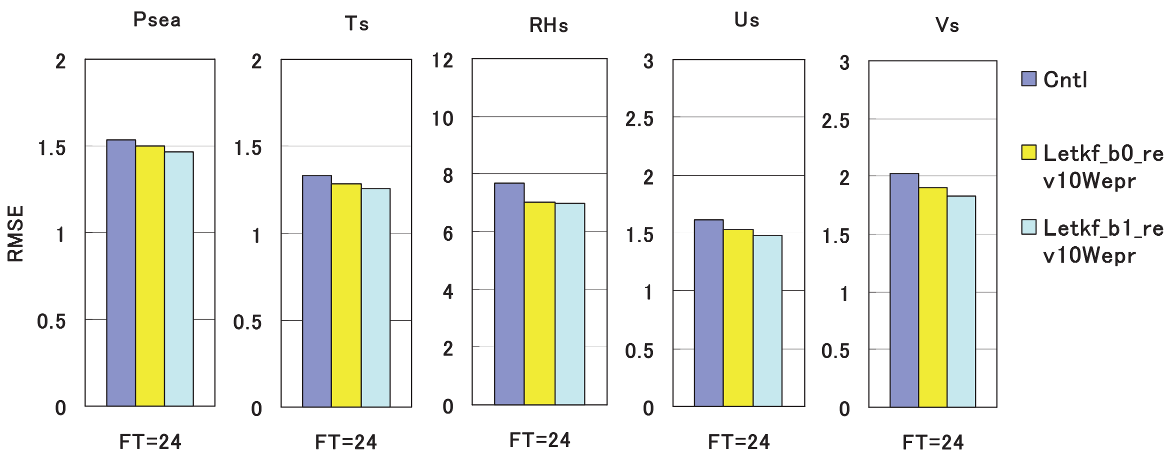

Fig. E-5-24. Averaged RMSEs against initial conditions in the 2 days of 3 and 4 July 2008 for surface elements in the LET method. From left to right, mean sea level pressure, 2 m temperature, 2 m relative humidity, 10 m horizontal wind (U and V). Letkf_b0_rev10Wepr is lateral boundary perturbations in the forecast, and Letkf_b1_rev10Wepr is the result with lateral boundary perturbations both in the EnKF cycle and forecast.

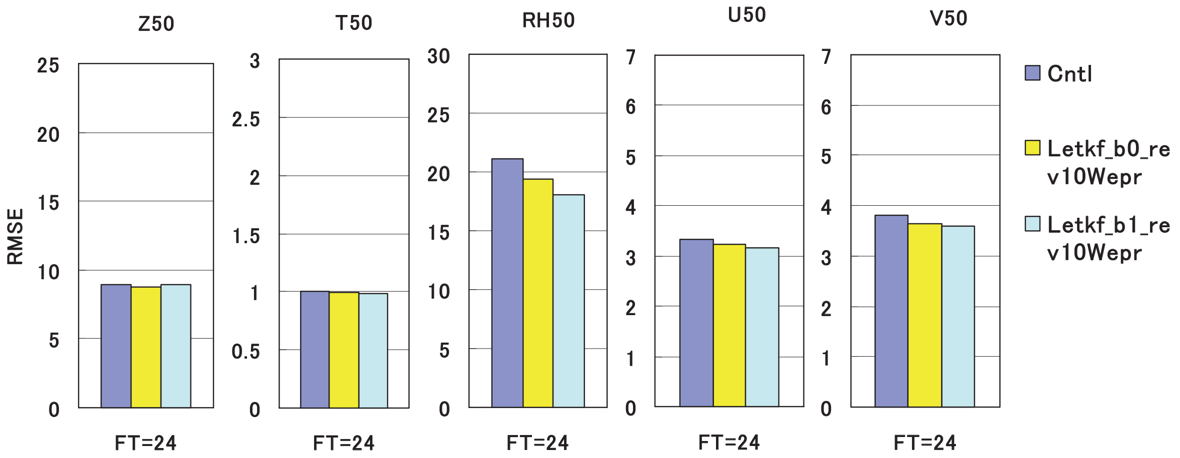

Fig. E-5-25. Same as in Fig. E-5-24 but elements at 500 hPa level.

c. Similarity index

As discussed in E-5-4e, similarity indexes of initial perturbations were checked for LET as well. Tables E-5-3 and E-5-4 show the similarity indexes for the cases of without and with lateral boundary perturbations in EnKF cycles, respectively. Orthogonalities between the initial perturbations are generally good, and unlike the MBD cases (Tables E-5-1 and E-5-2) they are not so affected by the implementation of lateral boundary perturbations in forecast analysis cycles. In other words, implementation of lateral boundary perturbations breeding cycle in MBD depends on the characteristics of the lateral boundary perturbation, whereas in LET, independency of transformed vectors does not rely on the orthogonality of the lateral boundary perturbation. In the case of LET, lateral boundary perturbations in EnKF cycles are important not to underestimate the forecast errors and to keep perturbation amplitude properly.

Table. E-5-3. Similarity index between LET initial perturbations. In case without lateral boundary perturbations in forecast analysis cycles.

	m1	m2	m3	m4	m5	m6	m7	m8	m9	m10
m1	1.00	0.07	−0.23	−0.18	0.01	0.09	−0.03	−0.46	−0.30	−0.19
m2	0.07	1.00	−0.11	−0.07	0.01	0.12	−0.31	−0.22	−0.33	−0.36
m3	−0.23	−0.11	1.00	−0.06	−0.40	−0.34	−0.12	−0.03	0.27	0.03
m4	−0.18	−0.07	−0.06	1.00	−0.22	−0.23	−0.02	−0.11	0.03	−0.15
m5	0.01	0.01	−0.40	−0.22	1.00	0.06	−0.16	−0.01	−0.25	−0.02
m6	0.09	0.12	−0.34	−0.23	0.06	1.00	−0.11	−0.07	−0.36	−0.18
m7	−0.03	−0.31	−0.12	−0.02	−0.16	−0.11	1.00	−0.14	0.10	−0.07
m8	−0.46	−0.22	−0.03	−0.11	−0.01	−0.07	−0.14	1.00	0.00	0.11
m9	−0.30	−0.33	0.27	0.03	−0.25	−0.36	0.10	0.00	1.00	−0.02
m10	−0.19	−0.36	0.03	−0.15	−0.02	−0.18	−0.07	0.11	−0.02	1.00

Table. E-5-4. Same as Table E-5-3. In case with lateral boundary perturbations in forecast analysis cycles.

	m1	m2	m3	m4	m5	m6	m7	m8	m9	m10
m1	1.00	−0.10	0.19	−0.18	−0.10	−0.56	−0.01	0.03	−0.02	−0.23
m2	−0.10	1.00	−0.51	−0.25	0.32	0.12	−0.07	−0.14	−0.27	−0.07
m3	0.19	−0.51	1.00	0.01	−0.37	−0.19	−0.07	0.07	0.09	−0.26
m4	−0.18	−0.25	0.01	1.00	−0.26	−0.02	−0.11	−0.10	−0.07	−0.03
m5	−0.10	0.32	−0.37	−0.26	1.00	0.06	−0.17	−0.17	−0.15	−0.14
m6	−0.56	0.12	−0.19	−0.02	0.06	1.00	−0.09	−0.17	−0.20	0.07
m7	−0.01	−0.07	−0.07	−0.11	−0.17	−0.09	1.00	−0.31	−0.20	0.00
m8	0.03	−0.14	0.07	−0.10	−0.17	−0.17	−0.31	1.00	−0.17	−0.22
m9	−0.02	−0.27	0.09	−0.07	−0.15	−0.20	−0.20	−0.17	1.00	0.04
m10	−0.23	−0.07	−0.26	−0.03	−0.14	0.07	0.00	−0.22	0.04	1.00

d. Effect of lateral boundary perturbations in EnKF cycles on accuracy of the LETKF analysis

In the former subsection, perturbations produced by the ensemble transform in LETKF were used only as the initial perturbations for a high resolution (15 km) extended run and the Meso 4DVAR analysis (E-3-1) gives the initial condition for the control run. NHM-LETKF makes its own analysis, but it was discarded for ensemble prediction. In case of LETKF, forecast errors are evaluated by the ensemble spread thus it seems that without lateral boundary perturbations, forecast errors near lateral boundaries are underestimated. This underestimation of forecast errors yields underestimation of the Kalman gain near lateral boundary and may affect accuracy of the LETKF analysis. To see the differences of analysis, we conducted additional experiments where LETKF analyses (ensemble mean) were used as the initial conditions of control runs.

Figure E-5-26 shows the evolution of ensemble spreads by the experiments without and with the lateral boundary perturbations in forecast-analysis cycles in LETKF. Similar tendencies are seen as in the case of Meso 4DAVAR analysis (Figs. E-5-19 and E-5-22), that is, ensemble spread grows more rapidly and diurnal changes in surface temperature and relative humidity become more distinct by the implementation of lateral boundary perturbations in EnKF cycles.

RMSEs of 24 hour forecast of LETKF analysis and ensemble mean against the initial condition the day after (Meso 4DVAR analysis) are shown in Figs. E-5-27 (surface) and E-5-28 (500 hPa).

At surface, RMSEs of the control run by LET (red bars) are larger than that by Meso 4DVAR (blue bars) except for V at surface. When the lateral boundary perturbations are implemented in EnKF forecast-analysis cycles, RMSEs of the control run decrease for RH and U, but increase for Psea and Ts. At 500 hPa level, RMSEs of the control run by LET are larger than that by Meso 4DVAR for T and U, while smaller for Z500. When the lateral boundary perturbations are implemented in EnKF cycles, RMSEs of control runs decrease for all variables. This result means that the accuracy of LETKF analysis improves with the implementation of lateral boundary perturbations in the EnKF analysis cycles. RMSEs of ensemble means are smaller than control runs for all variables at both surface and 500 hPa level.

Figures E-5-29 and E-5-30 show the control run and ensemble forecasts predicted by the LETKF analysis with lateral boundary perturbations in EnKF cycles. Despite the limitation of the number of ensemble member and assimilated observation data, forecast fields are seemingly not so inferior to the forecast from the Meso 4DVAR (Figs. E-5-2 and E-5-23).

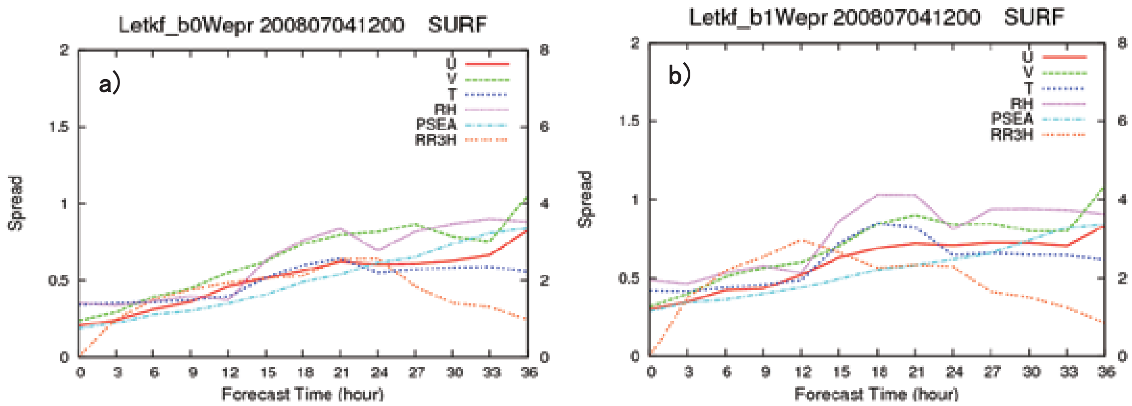

Fig. E-5-26. a) Same as Fig. E-5-19 but the control run was given by the LETKF analysis. b) Same as Fig. E-5-21 but the control run was given by the LETKF analysis with lateral boundary perturbations in EnKF cycles.

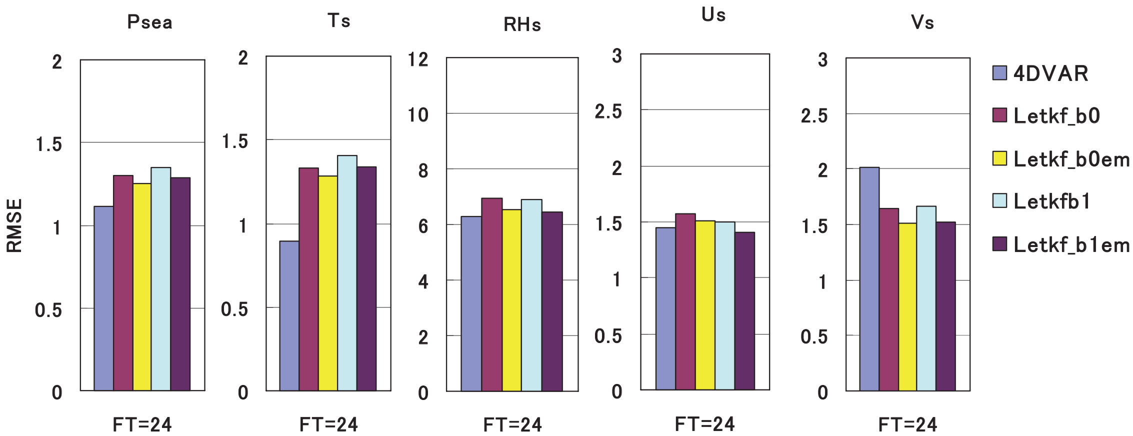

Fig. E-5-27. Averaged RMSEs of FT=24 forecast fields from 4 July 2008 against the Meso 4D-VAR analysis of 5 July 2008 for surface elements. From left to right, mean sea level pressure, 2 m temperature, 2 m relative humidity, 10 m horizontal wind (Us and Vs). Letkf_b0 and Letkfb0em are LETKF analysis and its ensemble mean without lateral boundary perturbations in EnKF cycles, respectively. Letkf_b1 and Letkf_b1em are LETKF analysis and its ensemble mean with lateral boundary perturbations in EnKF cycles.

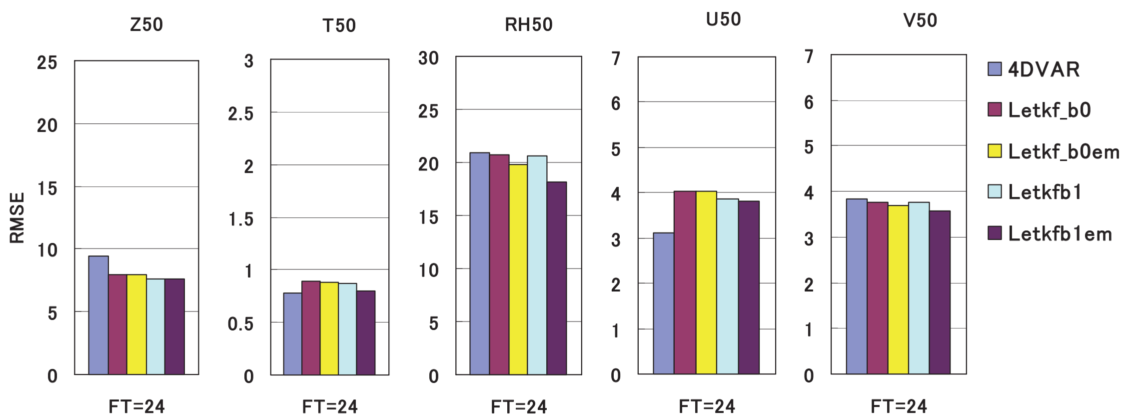

Fig. E-5-28. Same as in Fig. E-5-25 but elements at 500 hPa level.

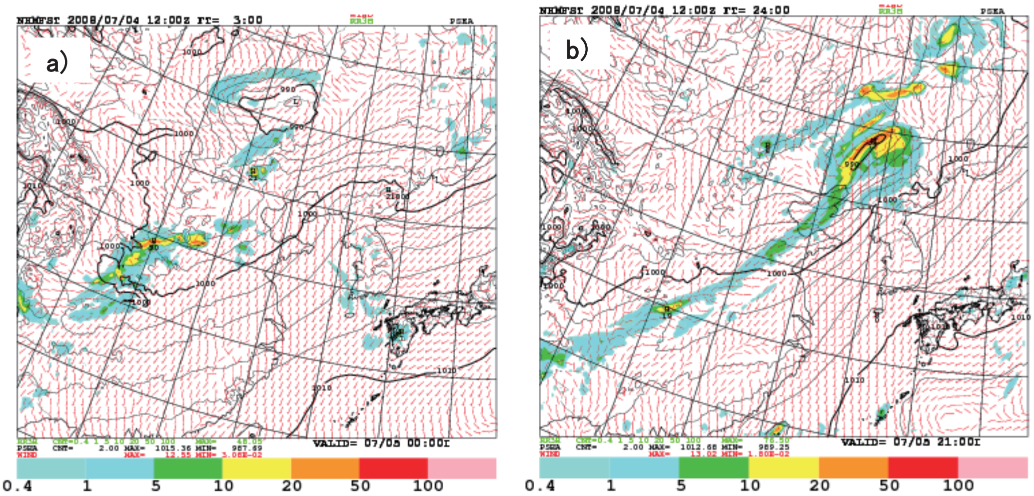

Fig. E-5-29. Same as in Fig. E-5-2 but initial condition is given by the LETKF analysis with lateral boundary conditions in EnKF cycles.

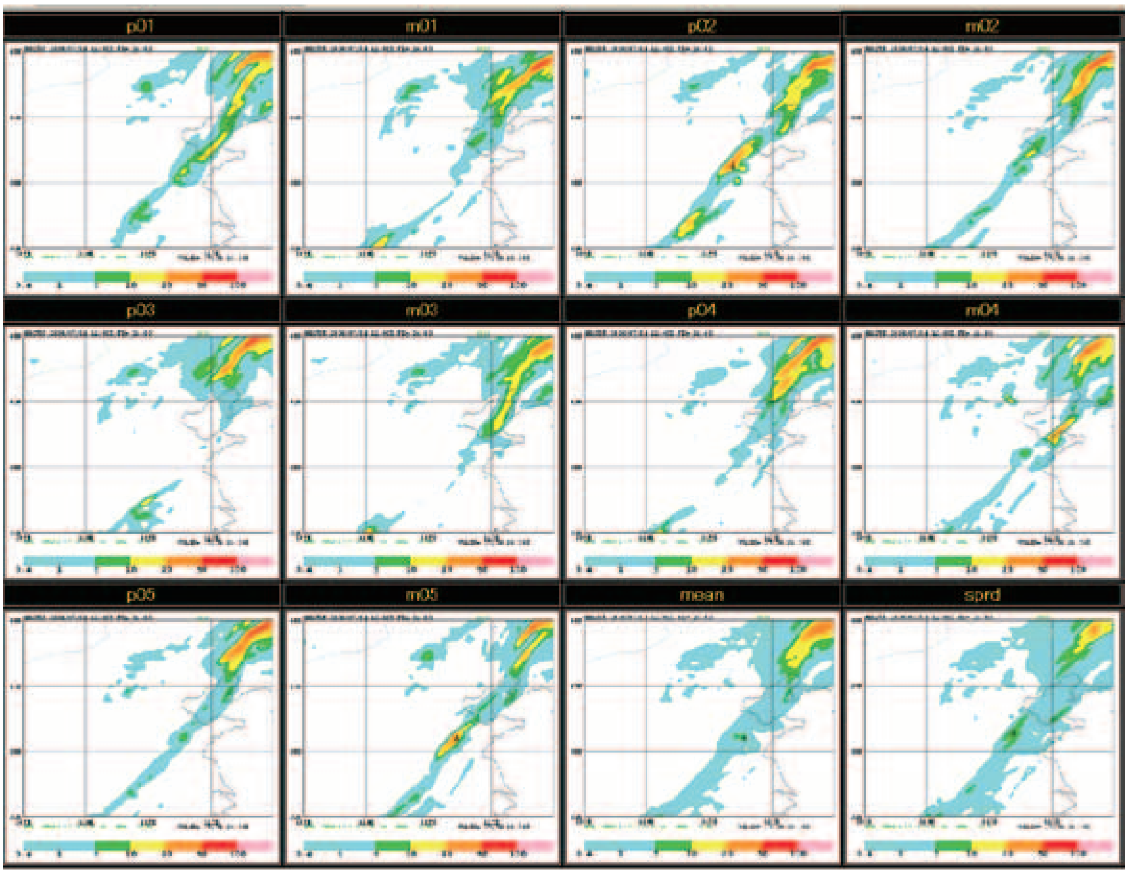

Fig. E-5-30. Same as in Fig. E-5-23 but initial condition is given by the LETKF analysis with lateral boundary conditions in EnKF cycles.